blood®
Regular Article

PLATELETS AND THROMBOPOIESIS

A zinc transporter, transmembrane protein 163, is critical for the biogenesis of platelet dense granules

Yefeng Yuan,[1,2] Teng Liu,[3,4] Xiahe Huang,[2] Yuanying Chen,[1] Weilin Zhang,[5] Ting Li,[2] Lin Yang,[2] Quan Chen,[5,6] Yingchun Wang,[2] Aihua Wei,[3] and Wei Li[1,4]

[1]Beijing Key Laboratory for Genetics of Birth Defects/Beijing Pediatric Research Institute, MOE Key Laboratory of Major Diseases in Children, Genetics and Birth Defects Control Center/National Center for Children's Health, and Beijing Children's Hospital/Capital Medical University, Beijing, China; [2]University of Chinese Academy of Sciences, Institute of Genetics and Developmental Biology, Chinese Academy of Sciences, Beijing, China; [3]Department of Dermatology, Beijing Tongren Hospital, Capital Medical University, Beijing, China; [4]Shunyi Women and Children's Hospital of Beijing Children's Hospital, Beijing, China; [5]State Key Laboratory of Membrane Biology, Institute of Zoology, Chinese Academy of Sciences, Beijing, China; and [6]Tianjin Key Laboratory of Protein Science, College of Life Sciences, Nankai University, Tianjin, China

KEY POINTS

- A zinc transporter, TMEM163, is essential for the biogenesis and function of platelet DGs.
- BLOC-1 complex is involved in the trafficking of TMEM163 to platelet DGs, which explains the defective DGs in HPS.

Lysosome-related organelles (LROs) are a category of secretory organelles enriched with ions such as calcium, which are maintained by ion transporters or channels. Homeostasis of these ions is important for LRO biogenesis and secretion. Hermansky-Pudlak syndrome (HPS) is a recessive disorder with defects in multiple LROs, typically platelet dense granules (DGs) and melanosomes. However, the underlying mechanism of DG deficiency is largely unknown. Using quantitative proteomics, we identified a previously unreported platelet zinc transporter, transmembrane protein 163 (TMEM163), which was significantly reduced in BLOC-1 (*Dtnbp1*^{sdy} and *Pldn*^{pa})–, BLOC-2 (*Hps6*^{ru})–, or AP-3 (*Ap3b1*^{pe})–deficient mice and HPS patients (HPS2, HPS3, HPS5, HPS6, or HPS9). We observed similar platelet DG defects and higher intracellular zinc accumulation in platelets of mice deficient in either TMEM163 or dysbindin (a BLOC-1 subunit). In addition, we discovered that BLOC-1 was required for the trafficking of TMEM163 to perinuclear DG and late endosome marker–positive compartments (likely DG precursors) in MEG-01 cells. Our results suggest that TMEM163 is critical for DG biogenesis and that BLOC-1 is required for the trafficking of TMEM163 to putative DG precursors. These new findings suggest that loss of TMEM163 function results in disruption of intracellular zinc homeostasis and provide insights into the pathogenesis of HPS or platelet storage pool deficiency. (*Blood*. 2021;137(13):1804-1817)

Introduction

Hermansky-Pudlak syndrome (HPS) is a recessive disorder featured by oculocutaneous albinism, prolonged bleeding, and ceroid deposition. It is also accompanied by lung fibrosis, colitis, and other complications in some cases.[1,2] The characteristic hallmarks of HPS are defects in multiple lysosome-related organelles (LROs), including dense granules (DGs) in platelets, melanosomes in melanocytes, Weibel-Palade bodies in endothelial cells, large-dense core vesicles in adrenal chromaffin cells, synaptic vesicles (SVs) in neurons, and lamellar bodies in alveolar type II epithelial cells.[2-6] LROs are regarded as a category of secretory organelles sharing properties with conventional lysosomes, such as highly glycosylated integral lysosome-associated membrane proteins (LAMPs) and enrichment of intralumenal ions such as calcium (Ca^{2+}).[2,3,7]

As inferred from melanosome biogenesis studies, platelet DGs are thought to originate via intermediary endosomes and multivesicular bodies (MVBs), and proteins may be transported to immature or mature DGs by a variety of protein complexes, such as the HPS protein–associated complexes (HPACs).[2,8-14] However, the underlying mechanisms whereby HPACs affect DG biogenesis remain uncharacterized. In addition, Rab32 and Rab38 regulate the transport of LAMP2 and VMAT2 (DG integral membrane protein) from early endosomes (EEs) to mepacrine positive compartments.[10,15] The Rab32 and Rab38 double mutant mimics severe HPS and has decreased DGs.[16] Rab32/Rab38 may not directly interact with these cargoes (eg, LAMP2 or VMAT2), and whether LAMP2 or VMAT2 deficiency causes defective DG biogenesis is unknown. Deficiency of SLC35D3 (a transmembrane protein) affects DG biogenesis,[17,18] but there is no clear evidence that SLC35D3 is localized to DGs. Altogether, the underlying mechanisms of DG biogenesis are largely unknown.

Traditionally, ion channels play a pivotal role in LRO biogenesis. Two-pore channel 2 (TPC2) regulates the pH, release of Ca^{2+}, membrane dynamics, and content exchange of mepacrine-positive compartments in MEG-01 cells.[19] In melanocytes, TPC2 regulates melanosomal pH and size by mediating Ca^{2+} release from

melanosomes, thus controlling pigmentation.[20] Our recent studies demonstrated that mitochondrial NCKX5 (a member of the K^+-dependent Na^+/Ca^{2+} exchanger family) participates in melanosome maturation and pigment production by regulating Ca^{2+} homeostasis of melanosomes.[21] Thus, similar to the melanosome, homeostasis of lumenal ions is important for DG biogenesis. However, knowledge of ion transporters in DGs is very limited.

Rats have an increased bleeding tendency upon maintenance on a Zn^{2+}-deficient diet.[22-24] In addition, a bleeding tendency along with abnormal platelet aggregation was noted in 2 cancer patients (one with squamous cell carcinoma and another with non-Hodgkin lymphoma) presenting with a nutritional Zn^{2+} deficiency. Normal bleeding times and platelet aggregation were restored by dietary zinc (Zn^{2+}) supplementation.[25] Zn^{2+} is known as a mediator of hemostasis.[26-30] Upon incubation with exogenous Zn^{2+}, platelets stained with the fluorescent Zn^{2+} indicator FluoZin-3 display a rapid fluorescence increase,[31] indicating that platelet Zn^{2+} entry pathways exist. It has been reported that intracellular Zn^{2+} homeostasis is maintained by 2 highly conserved Zn^{2+} transporter protein families, ZIP (SLC39) and ZNT (SLC30), in mammalian cells. The 14 members of ZIP protein family regulate influx of Zn^{2+} into the cytoplasm from the extracellular matrix and the lumen of vesicular compartments. By contrast, the 10 members of ZNT protein family regulate efflux of Zn^{2+} into the extracellular matrix and the lumen of vesicular compartments from the cytoplasm.[32-39] However, there is no report of Zn^{2+}-selective ion channels or transporters in platelets. Zn^{2+} has been proposed as an intracellular second messenger, analogous to Ca^{2+}, being released into the cytosol from intracellular storage pools.[40] However, the storage pools of Zn^{2+} in platelets have not been resolved.

In rat brain synaptosomes, transmembrane protein 163 (TMEM163), also called synaptic vesicle 31 (SV31), was first identified as a SV membrane protein binding Zn^{2+}.[41] Exogenously expressed rodent TMEM163 mainly localized to the plasma membrane, lysosomes, and SVs.[42-44] Purified rodent TMEM163 reconstituted in lipid bilayers assembles into a dimer and functions as a proton-dependent Zn^{2+} transporter.[45] In addition, TMEM163 interacts with transient receptor potential mucolipin-1 (TRPML1), which has been implicated in mucolipidosis type IV (MLIV) pathogenesis. Both fibroblasts of a MLIV patient and human embryonic kidney (HEK293) cells with knockdown of TRPML1 showed abnormal lysosomal Zn^{2+} accumulation.[43,44,46] Furthermore, TRPML1-deficient mice displayed increased Zn^{2+} levels in postmortem brain,[46] suggesting that TRPML1 and TMEM163 play critical roles in intracellular Zn^{2+} homeostasis. In the Indian population, TMEM163 is a genome-wide association study candidate gene associated with insulin resistance and type 2 diabetes.[47] Although, TMEM163 transcripts are detected in numerous tissues, including brain, kidney, lung, pancreas, testis, and ovary,[41,43] the function of TMEM163 is controversial,[43,48] and its presence, localization, and function in platelets are unknown.

In the present study, we find that TMEM163 is a critical component of the limiting membrane of the DG and late endosome (LE) marker–positive compartment (likely a precursor of DGs) in MEG-01 cells. TMEM163 is reduced in platelets of mice and HPS patients lacking HPACs (BLOC-1, BLOC-2 and AP-3). We demonstrate that BLOC-1 interacts with TMEM163 during its transport from EEs to perinuclear DG and LE marker–positive compartments. This may explain the similar DG defects in both *Tmem163* knockout mice and some of the above-mentioned HPS mutant mice.

Materials and methods

Mice

The sandy (*Dtnbp1*^{sdy}) mutant in the C57BL/6J background (wild-type [WT]) was originated from *sdy* mutant in the DBA/2J background[49] through backcrossing at least 8 generations. Other mouse mutants and their controls, including pallid (*Pldn*^{pa}), ruby-eye (*Hps6*^{ru}), pale-ear (*Hps1*^{ep}), pearl (*Ap3b1*^{pe}), buff (*Vps33a*^{bf}), a double mutant of ruby-eye and pale-ear (*ru/ep*), and a double mutant of buff and pale-ear (*bf/ep*) in the C57BL/6J background, were derived as described previously.[5,50] They were obtained from Richard T. Swank's laboratory at Roswell Park Comprehensive Cancer Center (Buffalo, NY). The *Tmem163* knockout mice (*Tmem163-KO*) were generated using Biosset's EGE system based on CRISPR-Cas9 in the C57BL/6J background. To ensure the genotypes of the littermates, polymerase chain reaction (PCR) amplifications were designed according to the targeted deletion of exons 1 and 2. All mice in this study were bred in the animal facility of the Institute of Genetics and Developmental Biology, Chinese Academy of Sciences. All procedures were approved by the Institutional Animal Care and Use Committee of the Institute of Genetics and Developmental Biology. Age-matched WT mice (C57BL/6J, B6) or heterozygous mice were used as background controls.

Human subjects

The 12 HPS1 to HPS6 patients (3 HPS1, 1 HPS2, 2 HPS3, 1 HPS4, 2 HPS5, and 3 HPS6) were identified in our group, and their clinical features and genotypes were described previously.[51] One HPS9 patient was identified recently.[52] Their parents were recruited in this study as controls. This study was approved by the internal review board of the bioethics committees of Beijing Tongren Hospital and Beijing Children's Hospital, Capital Medical University. The study followed the Declaration of Helsinki. Informed consent was signed by all subjects participating in this study. Peripheral blood samples (2 mL) were collected from all subjects for enrichment of platelets for immunoblotting.

Data analysis

All data were obtained from ≥3 independent experiments and expressed as mean ± standard error of the mean (SEM). All quantitative results were plotted by 1-way analysis of variance with Tukey's posttest, except where specified otherwise (eg, Student *t* test). Error bars indicate SEM (*$P < .05$; **$P < .01$; ***$P < .001$; N.S., not significant). All graphs were drawn in GraphPad Prism 5 (La Jolla, CA).

Details of additional materials and methods can be found in supplemental Data (available on the *Blood* Web site)

Results

TMEM163 expression in platelets is reduced in murine mutants and human patients of the HPS protein–associated complexes BLOC-1, BLOC-2, and AP-3

To investigate how HPACs function in DG biogenesis, we isolated the platelets of sandy (*sdy*; deficiency in BLOC-1 subunit

dysbindin) mice and their heterozygous littermates ($sdy^{+/-}$) for mass spectrometry. Using quantitative proteomics, we identified an uncharacterized transmembrane protein, TMEM163 (SV31), that was decreased in *sdy* mice compared with $sdy^{+/-}$ mice. The reduction of this protein is similar to CD63 (a type of DG integral membrane protein) (Figure 1A-B; supplemental Table 1; supplemental Figure 1). To verify the mass spectrometry results, we quantified endogenous TMEM163 protein expression in platelet lysates from *sdy* and $sdy^{+/-}$ mice by immunoblotting (Figure 1C). For comparison, we measured other lysates of platelets from BLOC-1–deficient pallid (*pa*) (Figure 1D), BLOC-2-deficient ruby-eye (*ru*) (Figure 1E), AP-3-deficient pearl (*pe*) (Figure 1F), and double mutant of ruby-eye and pale-ear (*ru/ep*) (Figure 1I) mice and their littermate controls. BLOC-1, BLOC-2, and AP-3 mutants showed significant reduction of TMEM163 relative to littermate control mice (Figure 1K). Interestingly, reduced TMEM163 in BLOC-1–, BLOC-2–, and AP-3–deficient platelets is similar to observations of reduced SLC35D3 in these mutant mice,[17] suggesting that both TMEM163 and SLC35D3 are likely transported by these HPACs. However, lysates of BLOC-3–deficient pale-ear (*ep*) (Figure 1G), buff (*bf*) with the $VPS33A^{D251E}$ mutation (Figure 1H), and double mutant of buff and pale-ear (*bf/ep*) (Figure 1J) mice showed no alteration of TMEM163 expression (Figure 1K). Consistently, 1 BLOC-1–deficient patient (1 HPS9), 7 BLOC-2–deficient patients (2 HPS3, 2 HPS5, and 3 HPS6), and 1 AP-3–deficient patient (1 HPS2) showed significant reductions of TMEM163 relative to healthy controls (Figure 1L-N). However, 4 BLOC-3–deficient patients (3 HPS1 and 1 HPS4) showed no alteration of TMEM163 expression (Figure 1M-N). These results agree with the finding that BLOC-1, BLOC-2, and AP-3 regulate cargo transport from endosomes to melanosomes in the same cargo-transport pathways in melanocytes,[11,12,50,53-56] whereas BLOC-3 and HOPS are involved in different routes in LRO biogenesis.[57] Altogether, these results indicate that TMEM163 may function in platelets and that BLOC-1, BLOC-2, and AP-3 may regulate the transport of TMEM163 to platelet LROs.

TMEM163 localizes to perinuclear DG and LE marker–positive compartments and EE-like organelles

Platelet α granules (AGs) and DGs are 2 major types of intracellular organelles that belong to the LRO family.[9] Due to lack of an applicable antibody for endogenous TMEM163 immunofluorescence staining, we used a human megakaryocytic cell line, MEG-01, to determine the localization of TMEM163.[8,10] MEG-01 cells were simultaneously transfected with different tagged-TMEM163 constructs (supplemental Figure 2), and we monitored Pearson correlation coefficients (PCCs) for the colocalization with multiple organelle markers. Confocal fluorescence microscopy revealed a high proportion of TMEM163 colocalization with platelet DG markers (Cherry-VMAT2, GFP-VMAT2, mepacrine, and CD63) (PCCs, 0.74 ± 0.04, 0.76 ± 0.02, 0.68 ± 0.04, and 0.73 ± 0.03, respectively) (Figure 2A-D,M), an LE marker (Rab7) (PCC, 0.72 ± 0.03) (Figure 2E), a lysosome marker (Lamp1) (PCC, 0.75 ± 0.02) (Figure 2F), and TPCN2 (likely in DG, LE or lysosome) (PCC, 0.59 ± 0.04) (Figure 2G). Consistently, live MEG-01 cells expressing Cherry-TMEM163 showed a high proportion of TMEM163 colocalization with LysoSensor Green DND-189 (PCC, 0.82 ± 0.02) (Figure 2H).[58] Therefore, TMEM163 is concentrated in acidic perinuclear DG and LE marker–positive compartments. Further analysis showed epitope-tagged TMEM163 overlapped with EE markers, EEA1 (PCC, 0.40 ± 0.02) (Figure 2I) and Rab5 (PCC, 0.63 ± 0.03) (Figure 2J). The DG positive limiting membrane protein VMAT2 overlapped to only a small proportion with EEA1 (PCC, 0.14 ± 0.01) (supplemental Figure 3B) compared with mepacrine (PCC, 0.81 ± 0.02) (supplemental Figure 3A). Notably, TMEM163 showed very little colocalization with AG markers (P-selectin, von Willebrand factor [VWF], and PF4) (PCCs, 0.13 ± 0.02, 0.04 ± 0.01, and 0.08 ± 0.01, respectively) (Figure 2K-L; supplemental Figure 3C-D). Furthermore, sucrose density gradient centrifugation assays (Figure 2N) showed that TMEM163 fractionated in F3-F9. TMEM163 partially cofractionated with the EE marker EEA1 in F3 to F5, the LE marker Rab7 in F6 to F9, and the DG marker LAMP2 in F5 to F8, further indicating that TMEM163 is localized to endosomal structures. Together, these results suggest that TMEM163 localized mostly to perinuclear DG and LE marker–positive compartments (likely DG precursors) and small vesicular structures (likely EEs) in the periphery of MEG-01 cells. The localization of TMEM163 in EE-like and DG precursor-like compartments suggests that TMEM163 may traffic from EEs to DGs.

TMEM163 interacts with BLOC-1

The decreased level of TMEM163 in BLOC-1 mouse mutants (*sdy* and *pa*; Figure 1C-D) and an HPS9 patient (Figure 1M) suggests that BLOC-1 may be involved in the trafficking of TMEM163. To determine whether TMEM163 is a cargo of BLOC-1, we tested for possible physical interactions between TMEM163 and the BLOC-1 subunits dysbindin, pallidin, and BLOS1. Coimmunoprecipitation (co-IP) of endogenous proteins showed that dysbindin interacted with TMEM163 (Figure 3A-B). Consistently, due to the deficiencies of dysbindin or TMEM163 in *sdy* or *Tmem163-KO* mice platelets, neither the anti-dysbindin nor the anti-TMEM163 antibody precipitated TMEM163 or dysbindin compared with their positive controls (Figure 3C-D). Furthermore, we confirmed that Flag-dysbindin-1A and Flag-BLOS1 (one of the shared subunits of BLOC-1 and BORC) coprecipitated with Myc-TMEM163 by co-IP assays, but not Flag-KXD1 (1 subunit of BORC) (supplemental Figure 4A-D). Moreover, pallidin precipitated with TMEM163 in B6 mice but not in the *pa* mutant (supplemental Figure 4E). However, the separation of dysbindin in F1 to F8 suggests that dysbindin and TMEM163 do not reside in a tight complex (Figure 2N), implying that TMEM163 may be one of multiple DG proteins transported by BLOC-1. These results suggest that BLOC-1 interacts with TMEM163 during its transport from EEs to perinuclear DG and LE marker–positive compartments (likely DG precursors).

TMEM163 deficiency affects the biogenesis of platelet DGs

We further analyzed the morphological characteristics of *DTNBP1*- and *TMEM163*-deficient cell lines (*DTNBP1-KO* [*D1*, *D12*, and *D24*] and *TMEM163-KO* [*T20* and *T87*] stable cell lines constructed by the CRISPR-Cas9 system, as shown in supplemental Figure 5) by thin-section transmission electron microscopy (TEM). A large number of organelles were present in WT MEG-01 cells after induction with 100 nM TPA for 4 days, including round membranous organelles resembling EEs with less intraluminal contents, LEs with more intraluminal contents and MVBs with intraluminal vesicles. Numerous enlarged round membranous organelles resembling EEs with less intraluminal content increased significantly in *DTNBP1-KO* (*D1* and *D24*) and *TMEM163-KO* (*T20* and *T87*) MEG-01 cells (Figure 4A-C). These

Figure 1. TMEM163 is reduced in platelets from HPS mouse models and patients with deficiency of BLOC-1, BLOC-2, or AP-3, but not BLOC-3. (A-B) Quantitative protein identification using liquid chromatography-mass spectrometery (LC-MS) of whole-platelet lysates in *sdy* mice compared with $sdy^{+/-}$ mice (ctrl). A total of 195 proteins (listed in supplemental Table 1) were selected using the Student *t* test and quantified with high confidence ($P < .05$). Hierarchy clustering of the z-scored isobaric tag for relative and absolute quantitation (iTRAQ) ratio of *sdy* to $sdy^{+/-}$ was used to evaluate the reproducibility of the experiments (A). The expression of TMEM163 in the platelets of *sdy* mice showed significant reduction compared with $sdy^{+/-}$ mice (B). n = 3, $*P < .05$. (C-J) Immunoblotting analysis of TMEM163 in platelets isolated from control mice and congenic HPS mutant mouse platelets with antibodies to TMEM163 or actin (a loading control). The expression of TMEM163 in platelets of *sdy* (BLOC-1-deficient HPS7 mutant), *pa* (BLOC-1-deficient HPS9 mutant), *ru* (BLOC-2-deficient HPS6 mutant), *pe* (AP-3-deficient HPS2 mutant), and *ru/ep* (BLOC-3-deficient model) double-mutant mice (both BLOC-2 and BLOC-3-deficient model) are significantly reduced compared with control mice (C-F,I). The expression of TMEM163 in platelets of *ep*, *bf* (the $VPS33A^{D251E}$ mutation model), and *bf/ep* showed no significant change compared with control mice (G-H,J). (K) TMEM163 band intensities were measured from ≥4 pairs of mice, normalized to actin levels, and expressed as the percentage (mean ± SEM) of the mean normalized value for control mice. (L) Immunoblotting assays showed the reduced TMEM163 in BLOC-2–deficient patients (2 HPS3, 2 HPS5, and 3 HPS6) compared with the healthy control (father or mother of each patient). (M) Immunoblotting assays showed normal TMEM163 in BLOC-3–deficient patients (3 HPS1 and 1 HPS4) and reduced TMEM163 in an AP-3–deficient patient (1 HPS2) and BLOC-1 deficient patient (1 HPS9) compared with the healthy control (father or mother of each patient). (N) Quantitative analysis of the TMEM163 band intensities. Each bar represents the percentage (mean ± SEM) of the mean normalized value for healthy control from 3 independent experiments. $*P < .05$; $**P < .01$; $***P < .001$. ctrl, control; N.S., not significant.

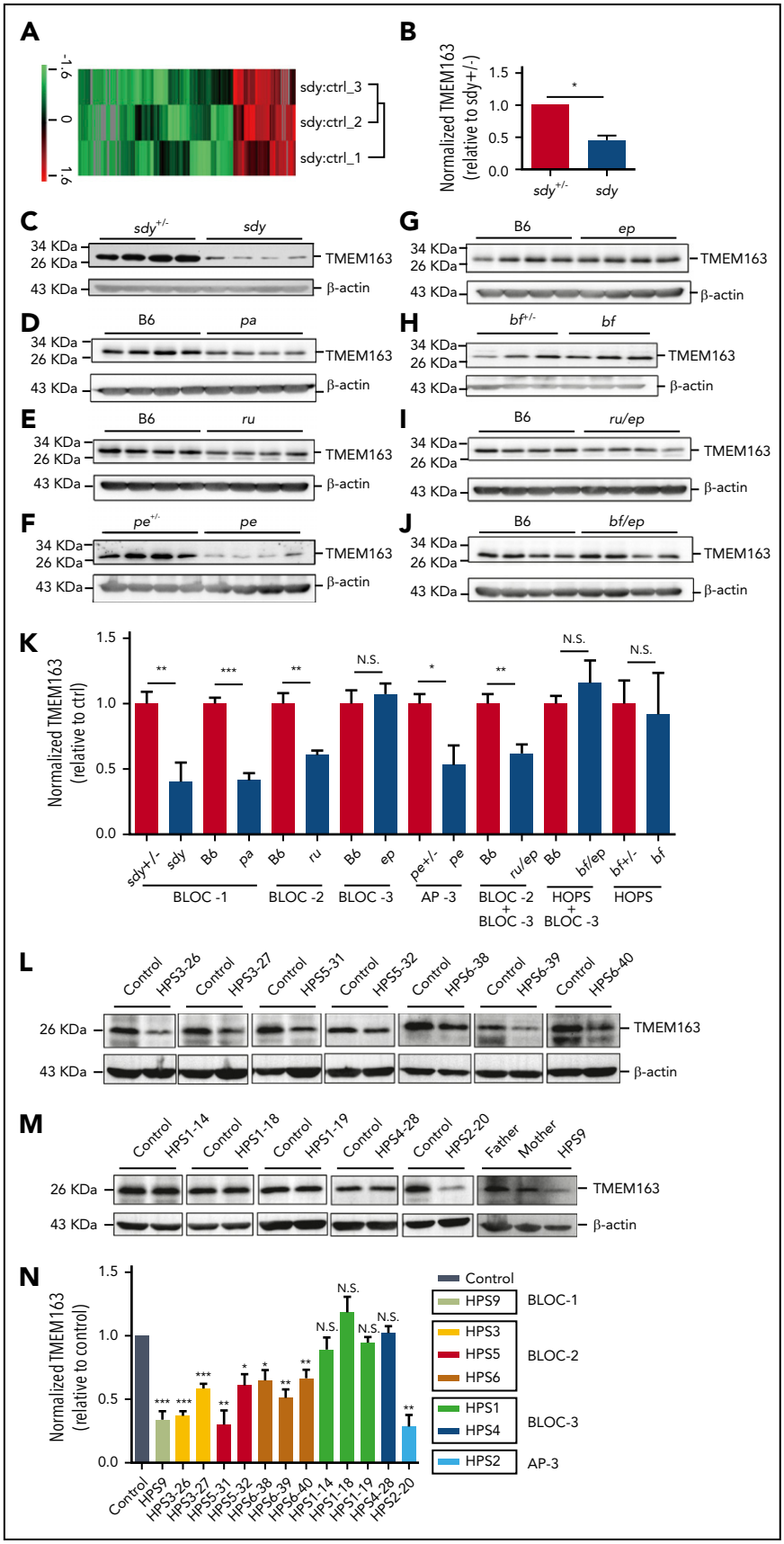

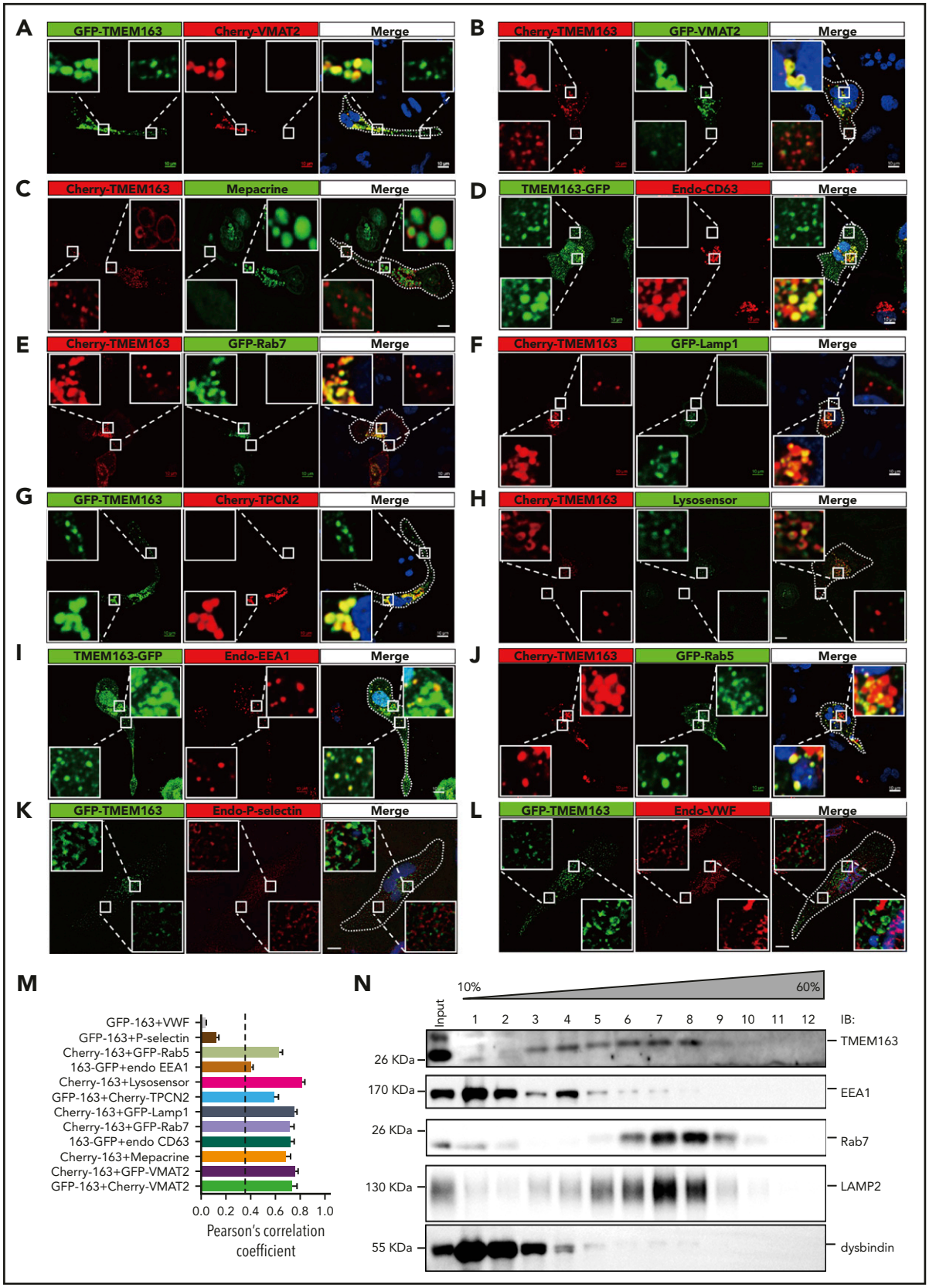

Figure 2. TMEM163 is localized to perinuclear DG and LE marker–positive compartments (likely DG precursors) and small vesicular structures (likely EEs) in the periphery, but not to AGs in MEG-01 cells. (A-B) MEG-01 cells were cotransfected with TMEM163-GFP or Cherry-TMEM163 and Cherry-VMAT2 (A) or GFP-VMAT2 (B) for 48 hours, respectively. (C) MEG-01 cells were transfected with Cherry-TMEM163 for 48 hours and then treated with 50 μM mepacrine for 30 minutes at 37°C. (D) MEG-01 cells were transfected with TMEM163-GFP for 48 hours and then fixed and stained with antibodies against CD63. (E-F) MEG-01 cells were cotransfected with Cherry-TMEM163 and GFP-Rab7 (E) or GFP-Lamp1 (F) for 48 hours, respectively. (G) MEG-01 cells were cotransfected with GFP-TMEM163 and Cherry-TPCN2 for 48 hours, respectively. (H) MEG-01 cells

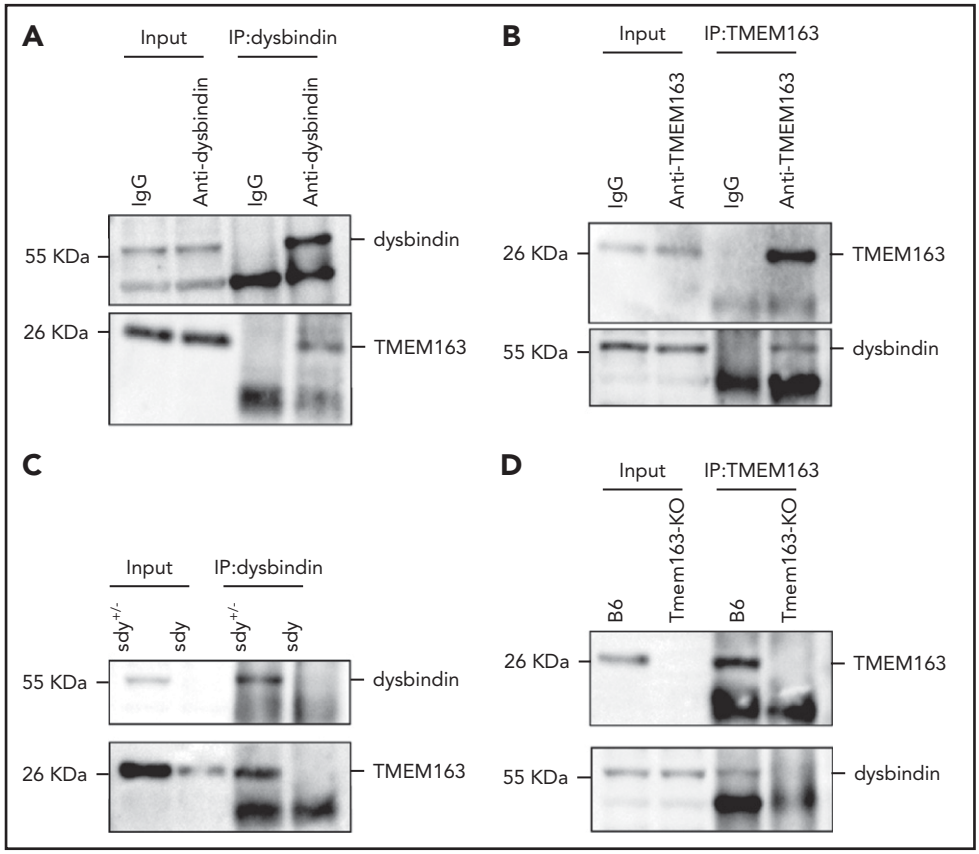

Figure 3. TMEM163 interacts with dysbindin. (A) Co-IP of endogenous platelet proteins show that dysbindin precipitates TMEM163. (B) Co-IP of endogenous platelet proteins show that TMEM163 precipitated dysbindin. The immunoglobulin G (IgG) was used as a negative control. (C) Co-IP of endogenous platelet proteins show that dysbindin precipitated TMEM163 in *sdy*$^{+/-}$ platelets, but not in *sdy* platelets. (D) Co-IP of endogenous platelet proteins show that TMEM163 precipitated dysbindin in WT (B6, C57BL/6J) platelets, but not in *Tmem163-KO* platelets. All the inputs corresponded to 8% of whole platelet lysates.

results suggest that deletion of dysbindin or TMEM163 resulted in the accumulation of large vacuoles.

We speculated that BLOC-1 participates in the biogenesis of DGs by regulating the transport of TMEM163 to DGs, and loss-of-function mutants of TMEM163 or BLOC-1 have similar phenotypes. To test this hypothesis, we constructed *Tmem163* knockout mice (*Tmem163-KO*) using the CRISPR-Cas9 system (supplemental Figure 6A-B). Both the tail genomic PCR and western blotting assays proved that the *Tmem163* gene was successfully deleted (supplemental Figure 6C-E). Through whole-mount TEM experiments, which has been used as the gold standard method for diagnosing platelet DG deficiencies,[59-62] we found that DGs in *Tmem163-KO* mice were absent, which is similar to *sdy* (C57BL/6J) mice (Figure 4D-E), suggesting that TMEM163 deficiency likely affects the biogenesis of platelet DGs.

Tmem163-KO (n = 6) and C57BL/6J (B6) (n = 8) mice did not differ significantly in platelet count, mean platelet volume, and other hematological parameters (supplemental Table 2). We observed no abnormalities in the surface expression of CD41, CD42b (GPIbα), and GPVI in *sdy* and *Tmem163-KO* platelets compared with their controls (supplemental Figure 7).

DGs concentrate small molecules such as serotonin, adenosine 5′-diphosphate (ADP), and Ca^{2+}.[63,64] Consistently, similar to *sdy* mutant, *Tmem163-KO* platelets displayed reduced ADP (Figure 4F) and serotonin (Figure 4G) relative to their littermate controls. Mepacrine, a green fluorescent dye, has a high affinity for adenine nucleotides and can be taken up by platelet DGs rapidly and selectively. Platelets of HPS patients have a significantly reduced uptake of mepacrine into DGs.[65-67] Similar to platelets of *sdy* mice, *Tmem163-KO* mouse platelets displayed significantly deficient uptake of mepacrine relative to platelets of littermate controls with a high dose of mepacrine (1.7 μM) (Figure 4H). In addition, we noticed that the defects in serotonin storage and mepacrine uptake were less profound in *Tmem163-KO* platelets than in *sdy* platelets, suggesting that TMEM163 plays a more specific role in DG biogenesis than BLOC-1 does.

Furthermore, we analyzed the ultrastructure of organelles in platelets of *Tmem163-KO, sdy* and *pa* (another BLOC-1 mutant[68]) mice. Based on the density of the dense core of round membranous compartments, the organelles of B6 mouse platelets were divided into 2 types; type I has low electron density (average gray value >50), and type II has a higher electron density (average gray value <50) (supplemental Figure 8F). Statistical

Figure 2 (continued) were transfected with Cherry-TMEM163 for 48 hours and treated with LysoSensor Green DND-189 for 30 minutes at 37°C. (I) MEG-01 cells were transfected with TMEM163-GFP for 48 hours and then fixed and stained with antibodies against EEA1. (J) MEG-01 cells were cotransfected with Cherry-TMEM163 and GFP-Rab5 for 48 hours. (K-L) MEG-01 cells were transfected with GFP-TMEM163 for 48 hours and then fixed and stained with antibodies against P-selectin (K) or VWF (L). Pictures shown in panels A-L are representative confocal images. Outlines of cells are indicated by white lines. Insets show 5× magnified images of the boxed region. Scale bars, 10 μm. (M) Colocalization analysis of results shown in panels A-L; PCC, 0.74 ± 0.04, 0.76 ± 0.02, 0.68 ± 0.04, 0.73 ± 0.03, 0.72 ± 0.03, 0.75 ± 0.02, 0.59 ± 0.04, 0.82 ± 0.02, 0.40 ± 0.02, 0.63 ± 0.03, 0.13 ± 0.02, and 0.04 ± 0.01; n = 11, 14, 8, 17, 7, 14, 13, 15, 22, 19, 10, and 10 cells, respectively. PCC ≥0.4 (dotted line) represents colocalization. (N) Sucrose (10% to 60%) gradient assay shows that TMEM163 coexists with the EE marker EEA1, the LE marker Rab7, and the DG marker LAMP2. Endo, endogenous; IB, immunoblotting.

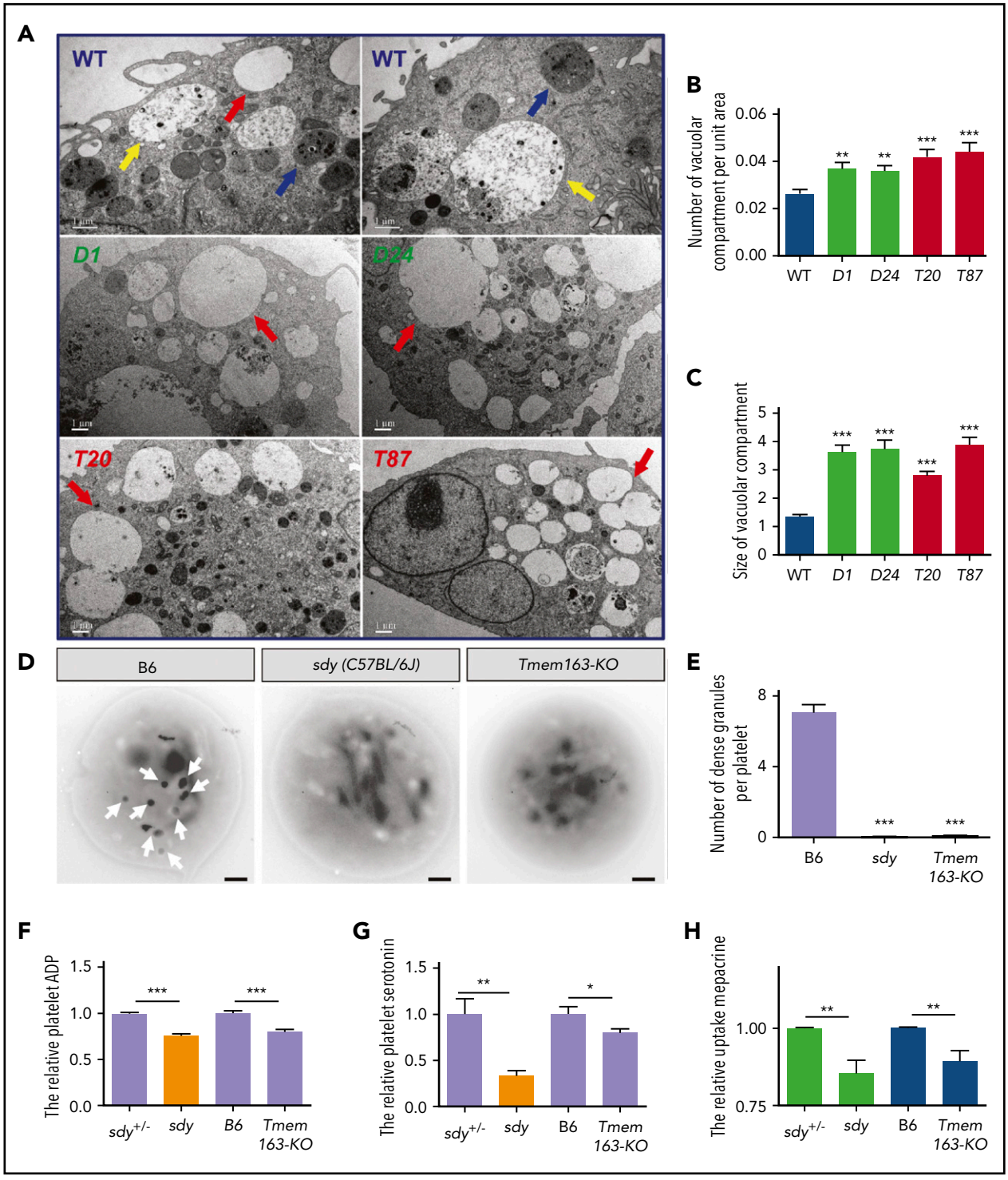

Figure 4. Ultrastructures of DGs in MEG-01 cells and platelets with deficiencies in dysbindin or TMEM163. (A) Thin-section TEM pictures of *DTNBP1-KO* (*D1* and *D24*) and *TMEM163-KO* (*T20* and *T87*) MEG-01 cells after induction with 100 nM TPA for 4 days. Red arrows represent round membranous organelles resembling EEs with reduced intraluminal contents, yellow arrows represent round membranous organelles resembling LEs with increased intraluminal contents, and blue arrows represent MVB circular membranous organelles. Scale bars, 1 μm. (B) The average number of vacuolar compartment (red arrows shown in panel A) per unit area (μm^2) in *DTNBP1-KO* (*D1* and *D24*) and *TMEM163-KO* (*T20* and *T87*) MEG-01 cells are significantly higher than that in control (WT) cells (WT, 0.027 ± 0.002, n = 47; *D1*, 0.037 ± 0.003, n = 48; *D24*, 0.036 ± 0.002, n = 52; *T20*, 0.042 ± 0.003, n = 55; *T87*, 0.044 ± 0.004, n = 40). (C) The average size of the vacuolar compartment (μm^2) in *DTNBP1-KO* (*D1* and *D24*) and *TMEM163-KO* (*T20* and *T87*) MEG-01 cells is significantly larger than that in WT cells (WT, 1.343 ± 0.080, n = 158; *D1*, 3.637 ± 0.234, n = 299; *D24*, 3.736 ± 0.302, n = 273; *T20*, 2.791 ± 0.145, n = 382; *T87*, 3.890 ± 0.245, n = 304). (D-E) TEM pictures of whole-mount platelets of the B6 (WT, C57BL/6J), *sdy* mutant, and *Tmem163-KO* mice. Arrows show platelet DGs. Lighter-intensity dots or smaller dots (diameter <100 nm) are not counted as DGs. Scale bars, 0.5 μm. DGs are absent in *sdy* (0.029 ± 0.020, n = 69) and *Tmem163-KO* (0.095 ± 0.020, n = 222) mice compared with B6 (7.069 ± 0.451, n = 58). (F-G) Washed platelets were lysed by 100 μL ice-cold lysis buffer, and the lysates used for further enzyme-linked immunosorbent assay were analyzed spectrophotometrically at 450 nm. The content of platelet ADP (*sdy* vs *Tmem163-KO*, 75.71% vs 79.77%, n = 4, 13, respectively) (F) and serotonin (*sdy* vs *Tmem163-KO*, 33.01% vs 79.51%, n = 6, 10, respectively) (G) of *sdy*, *Tmem163-KO* mice were calculated and plotted relative to their control littermates ($sdy^{+/-}$ or B6). (H) Platelets were incubated with 1.7 μM mepacrine at 37°C for 30 minutes and then analyzed by flow cytometry. The mepacrine uptake (green) fluorescence of *sdy* and *Tmem163-KO* was expressed as the percentage (mean ± SEM) of the mean normalized value for control mice (*sdy* vs *Tmeme163-KO*, 85.41% vs 89.29%, n = 9, 8, respectively). *$P < .05$; **$P < .01$; ***$P < .001$.

analysis of type I and type II compartments in *Tmem163-KO*, *sdy* and *pa* mutant mice, and their corresponding control mice, showed that *Tmem163-KO*, *sdy* and *pa* mutant mice displayed an abnormal type I accumulation and decreased type II compartments (supplemental Figure 8A-E,G-J). We speculate that the type I compartment represents an immature DG and the type II compartment represents a mature DG. This requires further confirmation by future immunogold labeling assays.

Moreover, *Tmem163-KO* platelets displayed normal steady-state levels of AG content and membrane proteins (basic fibroblast growth factor, endostatin, PF4, P-selectin, thrombospondin, and VWF) (supplemental Figure 9) and showed a significantly weaker endocytosis of fibrinogen (supplemental Figure 10), indicating that TMEM163 deficiency does not apparently affect the biogenesis of platelet AGs. Taken together, these results demonstrate that TMEM163 deficiency affects the biogenesis of platelet DGs, but not AGs. This finding is similar to that observed in BLOC-1 deficiency.

TMEM163 deficiency impairs platelet DG secretion

We next investigated possible roles of TMEM163 in the secretion of DGs by detecting adenosine triphosphate (ATP) release and in the secretion of AGs by measuring CD62p exposure and PF4 release. At various concentrations of collagen, *sdy* mutant and *Tmem163-KO* platelets both displayed significantly defective release of ATP compared with their littermate controls ($sdy^{+/-}$ or B6 mice) (Figure 5A; supplemental Table 3). Consistently, at various concentrations of thrombin (0.25, 1 U/mL), *sdy* mutant and *Tmem163-KO* platelets displayed significantly defective release of ATP (Figure 5B; supplemental Table 3). Both *sdy* and *Tmem163-KO* platelets showed impaired ATP release relative to controls in response to both collagen and thrombin. However, the defects in *Tmem163-KO* mice were milder than those in *sdy* mice, which is consistent with the milder serotonin storage and mepacrine uptake defects in the former, supporting that TMEM163 is one of multiple DG proteins transported by BLOC-1.

HPS6 deficiency displays impaired protein disulfide isomerase secretion and impaired exocytosis of AGs[69] and affects the tubulation and secretion of VWF.[70] Platelets from the HPS mutants pearl (*pe*), pallid (*pa*), and light ear (*le*) display impairment of AG secretion, which is regarded as secondary to deficient DG secretion.[71] Likewise, flow cytometry analysis demonstrated that *sdy* mutant and *Tmem163-KO* platelets displayed significant impairment of CD62p exposure at low doses of collagen (0.5 or 1.0 μg/mL) or thrombin (0.25 U/mL) compared with their littermate controls. Notably, the defects in *Tmem163-KO* mice were relatively milder than those in *sdy* mice. Impaired AG secretion could be rescued by high doses of agonists or exogenous ADP when there is no primary AG deficiency (Figure 5C-D; supplemental Figures 11 and 12). At higher doses of thrombin (0.5 U/mL) or with ADP supplement, CD62p levels revealed no significant differences (Figure 5C-D). Moreover, at various concentrations of collagen (0.8, 1.2, or 5 μg/mL) or at low doses of thrombin (0.25 U/mL), *sdy* mutant and *Tmem163-KO* platelets displayed significantly defective PF4 release. However, with a higher dose of thrombin (1 U/mL) or ADP supplement, there was no significant difference in PF4 release (Figure 5E-F). Taken together, both *sdy* and *Tmem163-KO* platelets showed impaired AG secretion relative to controls in response to both collagen and thrombin, suggesting that the impairment of AG secretion in *sdy* and *Tmem163-KO* platelets is secondary to deficient DG secretion and that there are no bona fide AG defects in both mutants.

TMEM163 deficiency impairs platelet function

To determine whether the defects of DG secretion resulted in abnormal platelet aggregation, we evaluated the aggregation of washed platelets from *sdy* and *Tmem163-KO* mice stimulated with various doses of agonists in a turbidimetric aggregometer. At different doses of collagen (1.2 or 2.4 μg/mL), *sdy* and *Tmem163-KO* mice showed significant impairment of platelet aggregation compared with their littermate controls (Figure 6A-B,E). Consistently, at different doses of thrombin (0.025 or 0.05 U/mL), *sdy* and *Tmem163-KO* mice showed significant impairment of platelet aggregation (Figure 6C-D,F). We further tested hemostasis in *Tmem163-KO* mice by recording tail-bleeding times. *Tmem163-KO* mice had significant prolongation in bleeding time (Figure 6G), suggesting that TMEM163 deficiency results in defective platelet aggregation and prolonged bleeding resembling the *sdy* mutant.

Tmem163-KO mice and HPS mouse mutants of BLOC-1, BLOC-2, and AP-3 show defective Zn^{2+} homeostasis

To further define the role of TMEM163 in the biogenesis of DGs, we investigated its function in megakaryocytes. TMEM163 has been shown to bind Zn^{2+} presumably as a proton-dependent Zn^{2+} transporter.[45] During blood clotting, activated platelets release a large amount of stored Zn^{2+} to the bloodstream.[31,72,73] Once platelets are stimulated, the 2 types of secretory granules (AGs and DGs) activate. AGs store protein-bound Zn^{2+},[74,75] but it is uncertain whether Zn^{2+} ions are present in DGs. When MEG-01 cells expressing Cherry-VMAT2 were treated with the Zn^{2+} indicator FluoZin-3, we found VMAT2-positive organelles enriched with FluoZin-3 dye (Figure 7A). Furthermore, we found that TMEM163 may act as a limiting membrane protein that packages FluoZin-3 dye (Figure 7B-C). These results suggest that perinuclear DG and LE marker–positive compartments (likely DG precursors) store free Zn^{2+}.

Next, we incubated *DTNBP1-KO* and *TMEM163-KO* cell lines with FluoZin-3 in the absence or presence of 100 μM $ZnCl_2$. We observed higher intracellular Zn^{2+} accumulation in granule-like structures of *DTNBP1-KO* (*D1*, *D24*) and *TMEM163-KO* (*T20*, *T87*) MEG-01 cells (supplemental Figure 13). In addition, washed platelets from *sdy* and *Tmem163-KO* mice also showed higher Zn^{2+} accumulation compared with platelets of their littermate controls under resting conditions. Similarly, the resting platelets of other HPS mouse models of BLOC-1 (*pa*), BLOC-2 (*ru*), and AP-3 (*pe*) mice showed higher Zn^{2+} accumulation (Figure 7D), consistent with the decreased TMEM163 expression.

Once platelets are activated by thrombin, Zn^{2+} is rapidly released from granules. Our data displayed similar kinetics of decrease in platelet Zn^{2+} levels in all mutant and control mice after activation by thrombin (Figure 7E-H), suggesting that Zn^{2+} is mostly stored in thrombin-triggered releasable granules. However, Zn^{2+} in AP-3 (*pe*)–deficient mice did not decline to basal levels (Figure 7I). One explanation is that the amount of thrombin used in this assay was not sufficient to release the highly accumulated Zn^{2+} in *pe* mice, as the fold change in *pe* platelets was the highest among these mutant mice (Figure 7D).

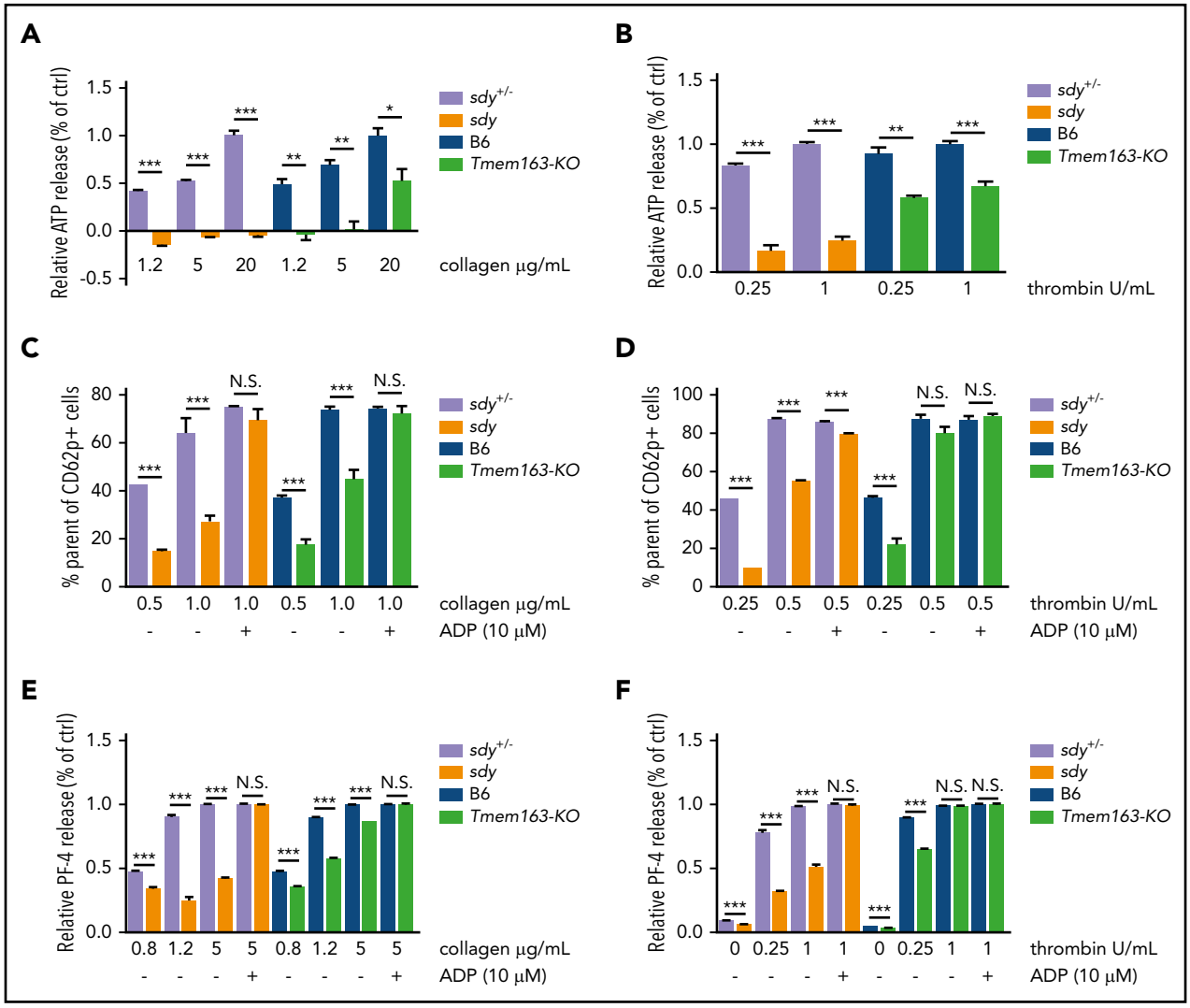

Figure 5. *Sdy* and *Tmem163-KO* platelets display significant impairment of DG release and AG secretion. (A-B) Washed platelets from *sdy*$^{+/-}$, *sdy*, B6 (WT, C57BL/6J) or *Tmem163-KO* mice were stimulated with various concentrations of collagen (1.2, 5, or 20 μg/mL) (A) or thrombin (0.25 or 1 U/mL) (B) and secretion of ATP assessed by ATP determination kit. Data represent the relative ATP release as the percentage (mean ± SEM) of the mean normalized value in maximal dose stimulation for their control mice. (C-D) Washed platelets from *sdy*$^{+/-}$, *sdy*, B6, or *Tmem163-KO* mice were labeled with fluorescein isothiocyanate-CD62p antibody and stimulated with various concentrations of collagen (0.5 or 1.0 μg/mL, *sdy* vs *Tmem163-KO*, n = 6, 6, respectively) (C) or thrombin (0.25 or 0.5 U/mL, *sdy* vs *Tmem163-KO*, n = 3, 6, respectively) (D) for 5 minutes in the absence or presence of 10 μM ADP and then measured by flow cytometry for CD62p surface expression. Data represent the percentage of platelets with labeling above the background level observed on unstimulated platelets. (E-F) Washed platelets from *sdy*$^{+/-}$, *sdy*, B6, or *Tmem163-KO* mice were stimulated with various concentrations of collagen (0.8, 1.2, or 5.0 μg/mL) (E) or thrombin (0, 0.25, or 1 U/mL) (F) for 5 minutes in the absence or presence of 10 μM ADP, and then supernatants were collected and measured by enzyme-linked immunosorbent assay for PF-4 (*sdy* vs *Tmem163-KO*, n = 4, 4, respectively.). Data shown represent the relative PF4 release as the percentage (mean ± SEM) of the mean normalized value in maximal dose stimulation for their control mice. *$P < .05$; **$P < .01$; ***$P < .001$.

Zn^{2+} accumulation in the platelets of these mutant mice may result from the defects in other Zn^{2+} transporters (ZnT/ZIP family members) residing in the organelles of platelets. However, our quantitative reverse transcription PCR results showed normal messenger RNA expression of ZnT (ZNT1, ZNT5, ZNT6, ZNT7, and ZNT9) and ZIP (ZIP1, ZIP4, ZIP6, ZIP7, ZIP9, and ZIP10) family members in mature megakaryocytes from *Tmem163-KO* mice relative to B6 mice (supplemental Figure 14). This suggests that TMEM163 deficiency may be the major contributor of Zn^{2+} accumulation in megakaryocytes and platelets.

Next, to explore whether decreasing Zn^{2+} accumulation in *sdy* and *Tmem163-KO* platelets would restore normal platelet aggregation, we incubated washed platelets with FluoZin-3 in the presence of a Zn^{2+} chelator, TPEN, and recorded the kinetics of aggregation during resting and activated states. Both resting and activated platelets of *sdy* and *Tmem163-KO* displayed reduced FluoZin-3 intensities with the addition of TPEN (supplemental Figure 15A-C), suggesting that TPEN effectively removes Zn^{2+} from platelets. We then incubated *sdy* and *Tmem163-KO* platelets with either 20 μM or 50 μM TPEN (dimethyl sulfoxide as a negative control). After stimulation with 0.05 U/mL thrombin, we found that TPEN inhibited platelet aggregation in a dose-dependent manner and did not restore the impairment of platelet aggregation in *sdy* and *Tmem163-KO* mice (supplemental Figure 15D-G), suggesting that the mutant defects occur in DG biogenesis, but not in DG secretion.

Taken together, these results demonstrate that deficiency of *DTNBP1* or *TMEM163* compromises intracellular organellar

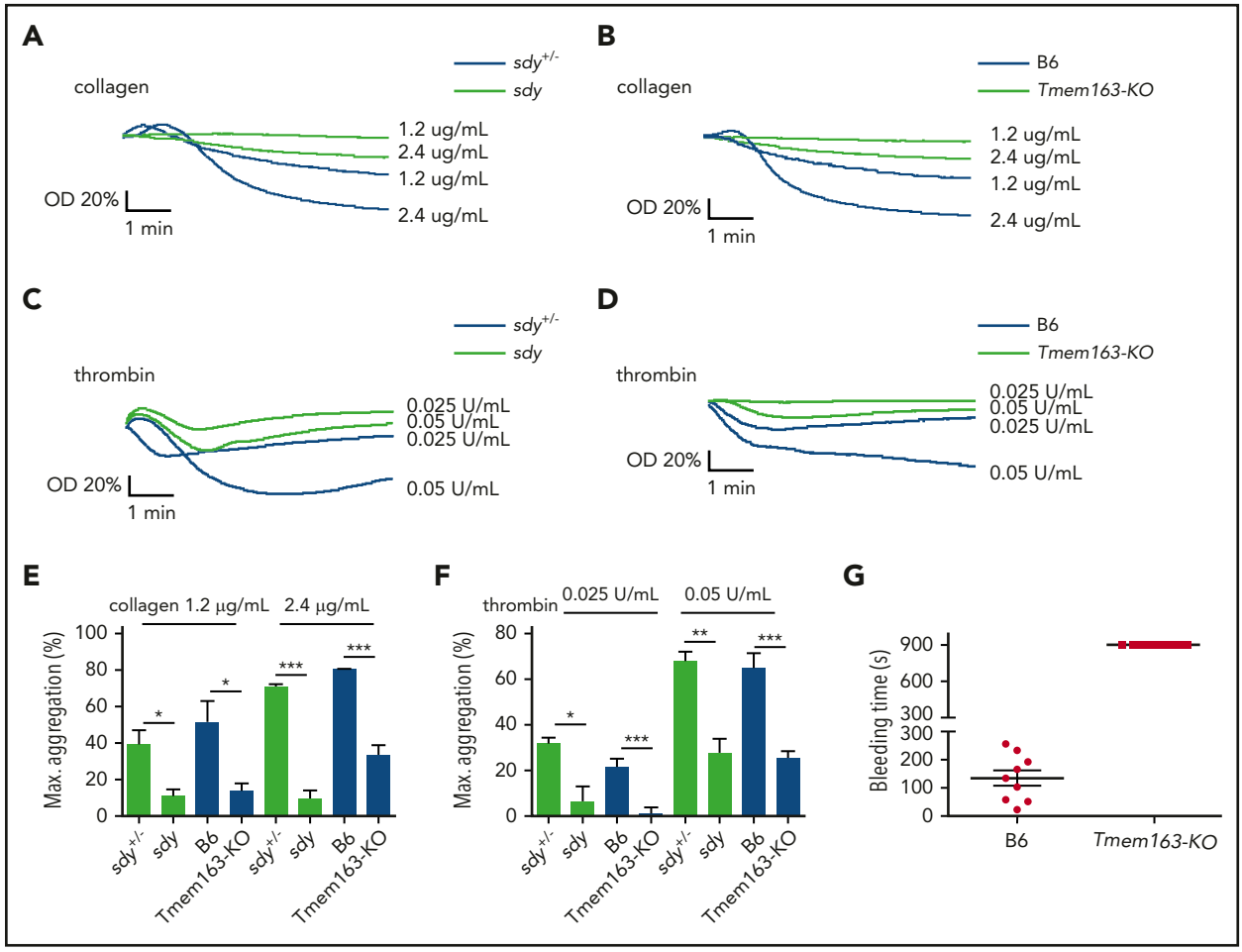

Figure 6. *Sdy* and *Tmem163-KO* display significant impairment of platelet aggregation and prolonged bleeding time. (A-F) Washed platelets from *sdy*$^{+/-}$, *sdy*, B6 (WT, C57BL/6J), or *Tmem163-KO* mice were stimulated with various concentrations of collagen (*sdy*$^{+/-}$ vs *sdy*, 39.38% vs 11.04% [1.2 µg/mL], and 71.05% vs 9.71% [2.4 µg/mL], n = 4, 4, 3, and 3, respectively; B6 vs *Tmem163-KO*, 51.50% vs 13.80% [1.2 µg/mL], and 80.42% vs 33.65% [2.4 µg/mL], n = 4, 4, 4, and 4, respectively) (A-B,E) or thrombin (*sdy*$^{+/-}$ vs *sdy*, 31.91% vs 6.53% [0.025 U/mL], and 68.03% vs 27.78% [0.05 U/mL], n = 4, 5, 3, and 3, respectively; B6 vs *Tmem163-KO*, 21.60% vs 0.99% [0.025 U/mL], 65.01% vs 25.44% [0.05 U/mL], n = 9, 7, 7, and 6, respectively) (C-D,F) and aggregation assessed by a turbidimetric aggregometer. (G) Tail-bleeding assays showed *Tmem163-KO* mice have prolonged bleeding times compared with B6 mice (B6, 135 ± 27.59 s; n = 9; *Tmem163-KO*, >900 s; n = 12). Student *t* test, **P* < .05; ***P* < .01; ****P* < .001. OD, optic density.

Zn^{2+} homeostasis in platelets and that defective Zn^{2+} homeostasis is highly correlated with DG biogenesis.

Discussion

Using different HPS mouse models and HPS patients, we identified a previously unreported DG Zn^{2+} transporter, TMEM163, which is significantly reduced in BLOC-1 (*sdy* and *pa*), BLOC-2 (*ru*), or AP-3 (*pe*) deficient mice and HPS patients (HPS2, HPS3, HPS5, HPS6, or HPS9). Furthermore, we determined that BLOC-1 interacts with TMEM163 during its transport from EEs to perinuclear DG and LE marker–positive compartments (likely DG precursors). Therefore, all of these mutant mice have defects in DG biogenesis and secretion, resulting in prolonged bleeding times and impaired platelet aggregation. Finally, similarly to the deficiency of BLOC-1, BLOC-2, or AP-3, which results in abnormal platelet intracellular organellar Zn^{2+} homeostasis of platelets, TMEM163 deficiency alters platelet Zn^{2+} homeostasis. These new findings are important for understanding the LRO defects in HPS and platelet storage pool deficiency.

From studies on melanosomes, it is reasonable to propose that HPACs are involved in platelet DG biogenesis by regulating the trafficking of multiple DG cargoes. In this study, we identified a novel membrane protein (likely a DG membrane protein), TMEM163, which interacts with BLOC-1 and is one of the multiple DG proteins transported by BLOC-1. Notably, our data demonstrated that TMEM163 was partially localized to EEs and was deficient in BLOC-1, BLOC-2, or AP-3 mutant mice but at normal levels in BLOC-3 or HOPS mutant mice. There are reports that in melanocytes and neurons, BLOC-1 and AP-3 act upstream of BLOC-2 in cargo trafficking, whereas BLOC-3 and HOPS act in different trafficking pathways.[1,2,76] Although it has been reported that RAB32 and RAB38 are required for the biogenesis of DGs,[10,16] both the expression of Rab32 and Rab38 in the platelets of *Tmem163-KO* mice showed no significant changes compared with their control mice (supplemental Figure 16). In addition, it has been reported that BLOC-1 physically interacts with BLOC-2 or AP-3 to facilitate TYRP1 trafficking from endosomes to melanosomes.[12] Our results suggest that BLOC-1, BLOC-2, and AP-3 are functionally required for TMEM163 transport, similar to some cargoes of melanosomes[57,77] and SVs.[78,79]

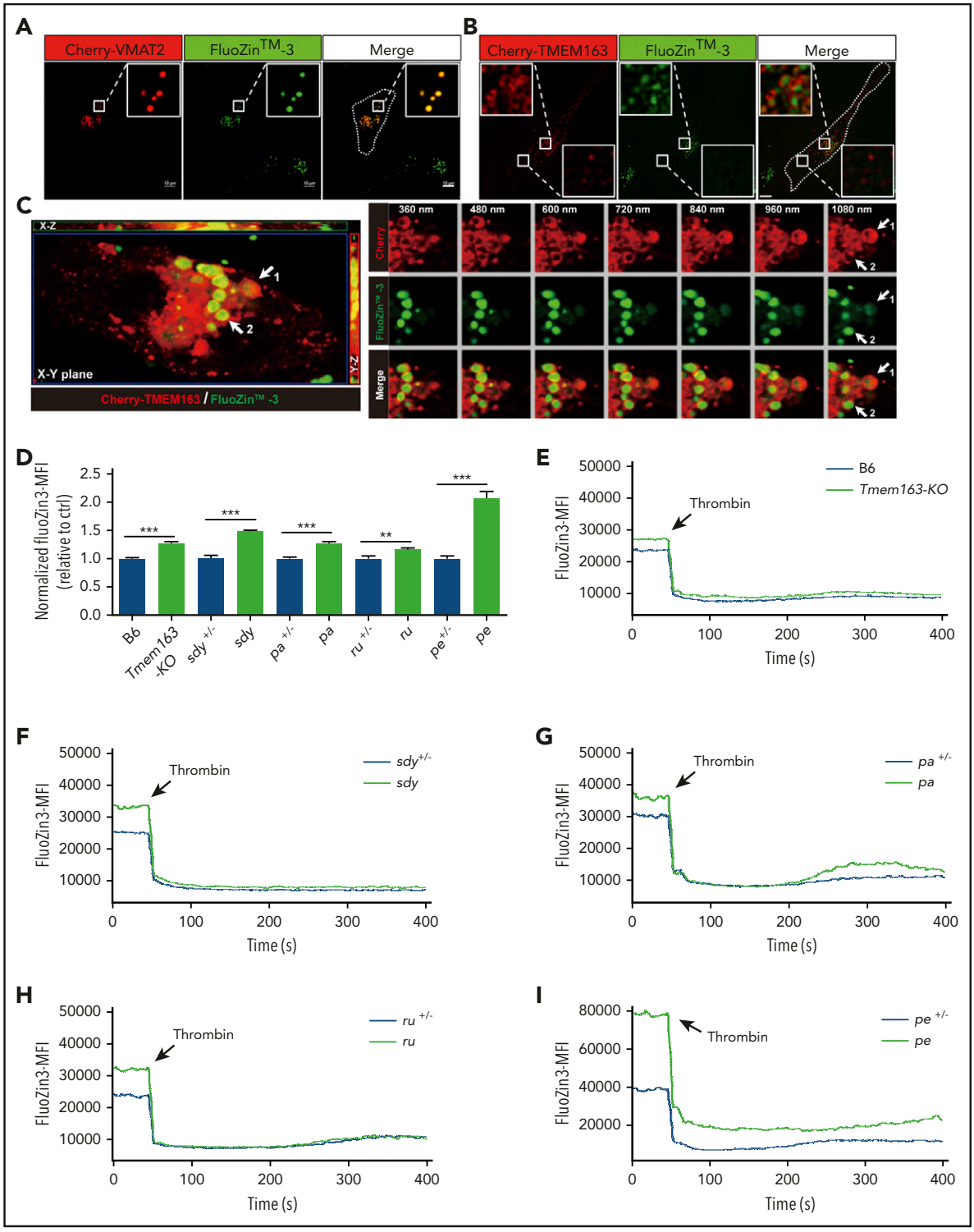

Figure 7. Defective Zn^{2+} homeostasis in platelets from *Tmem163-KO* mice and HPS mouse models of BLOC-1, BLOC-2 and AP-3. (A-B) MEG-01 cells were transfected with Cherry-VMAT2 (A) or Cherry-TMEM163 (B) for 48 hours then incubated with 2 μM Zn^{2+} indicator (FluoZin-3) for 30 minutes at 37°C. Pictures are representative confocal images. Outline of the cell is indicated by the white line. Insets show 5× magnified images of the boxed region. Scale bars, 10 μm. (C) MEG-01 cells were transfected with Cherry-TMEM163 for 48 hours and then incubated with 2 μM Zn^{2+} indicator (FluoZin-3) for 30 minutes at 37°C. Picture (left) is representative maximum intensity projection image in X-Y, X-Z, and Y-Z planes. Pictures (right) are Z-stack images in different dimensions. The arrows represent the classical colocalization of Cherrry-TMEM163 with FluoZin-3. (D-I) Washed mutant and control mice platelets were incubated with 2.5 μM FluoZin-3 and stimulated with 0.01 U/mL thrombin, and the kinetic curve of fluorescence changes was recorded by flow cytometry (appending the first 50 seconds [resting stage] to 400 seconds [activated stage]). Data shown are the quantitative results (D) of normalized FluoZin3 mean fluorescence intensity relative to each control at resting conditions and representative kinetic curves of Zn^{2+} release after thrombin treatment (E-I). B6 vs *Tmem163-KO*, n = 11, 11; $sdy^{+/-}$ vs *sdy*, n = 10, 10; $pa^{+/-}$ vs *pa*, n = 12; 12, $ru^{+/-}$ vs *ru*, n = 12, 12; and $pe^{+/-}$ vs *pe*, n = 12, 12, respectively. MFI, mean fluorescence intensity. Mean ± SEM, $^{**}P < .01$; $^{***}P < .001$.

Several other DG integral membrane proteins such as LAMP2, CD63, and VMAT2[10,19] have been identified, but the possible involvement of these proteins in DG biogenesis is unknown. However, the substantial combined evidence of whole-mount TEM, thin-section TEM, and DG contents presented here strongly support the critical involvement of TMEM163 in DG biogenesis. In summary, our data are consistent with a role of HPACs in the biogenesis of LROs, in which BLOC-1, BLOC-2, and AP-3 function in trafficking of TMEM163 from endosomes to perinuclear DG and LE marker–positive compartments (likely DG precursors). Considering that TMEM163 is specifically deficient in BLOC-1, BLOC-2, or AP-3 mouse models and HPS patients, we propose that TMEM163 or platelet Zn^{2+} concentration could be a new marker for the diagnosis and genotyping of HPS subtypes.

Platelet whole-mount TEM has long been the gold standard method for diagnosing platelet DG deficiencies.[59-62] As expected, *Tmem163-KO* platelets showed the typical "DG null" phenotype by this procedure. Interestingly, through thin-section TEM of platelets, we found that a deficiency of TMEM163, dysbindin, or pallidin causes the accumulation of the type I compartment (likely immature DGs) and a decrease in the type II compartment (likely mature DGs), which requires further future confirmation by immunogold labeling assays. Further analysis by thin-section TEM showed both *DTNBP1-KO* and *TMEM163-KO* MEG-01 cell lines have increased enlarged vacuoles, which may represent immature DGs or DG precursors in megakaryocytes. However, the underlying mechanisms of DG maturation during megakaryocyte differentiation require further investigation.

A previous report demonstrated that TMEM163 lies within the limiting membrane of SVs.[41] Both SVs and DGs belong to LROs.[2] It has been reported that TRPML1 interacts with TMEM163 to regulate the trafficking of TMEM163 from the plasma membrane to endocytic compartments, lysosomes, or SVs. TMEM163 was proposed as a zinc (Zn^{2+})/proton (H^+) exchanger and as a co-operative ionic channel with TRPML1 in lysosomes. TMEM163 functions in influxing Zn^{2+} into the cytoplasm from the extracellular matrix and the lumen of vesicular compartments,[43,44] indicating that TMEM163 acts as a ZIP protein and not as a ZNT protein. However, another study reported that TMEM163 effluxes Zn^{2+} from the cytosol. Thus, TMEM163 was designated as ZNT11, a new member of the ZNT family.[48] When SV31 is reconstituted in liposomes, TMEM163 assembles into a dimer and functions as a proton-dependent Zn^{2+} transporter, similar to ZNT3.[45] Our investigation indicated that deficiency of TMEM163 results in abnormally high intracellular Zn^{2+} content (accumulation in granule-like structures), thus affecting the biogenesis and function of DGs. We speculate that TMEM163 acts as a ZIP protein on DGs as Zn^{2+} is accumulated in granule-like structures when TMEM163 is deficient (Figure 7). Accumulated Zn^{2+} in platelets with a TMEM163 deficiency (or BLOC-1, BLOC-2, or AP-3 deficiency) may disrupt the ion homeostasis that is essential for DG biogenesis and secretion.

Acknowledgments

The authors thank Richard T. Swank, who provided the mutant mice in this study and proofread the manuscript; Runlin Z. Ma, who provided the pSpCas9 (BB)-2A-GFP (PX458) vector; Fangyuan Nie, who helped to analyze quantitative reverse transcription PCR data; and Chang Zhang, who provided the pEGFP-C2-Rab5, pEGFP-C2-Rab7, and pEGFP-C2-Lamp1 vectors. The authors thank Jiaying Yu, Jiran Lu, and Huipeng Wang for their help breeding several mutant mice.

This work was supported by grants from the Ministry of Science and Technology of China (2019YFA0802104) and the National Natural Science Foundation of China (31800977, 91954000, 31830054, 91539204, and 31900496).

Authorship

Contribution: Y.Y. and W.L. designed the research, analyzed the data and wrote the manuscript; Y.Y. performed most of the experiments; T. Liu and A.W. recruited all the subjects and collected the written informed consents; Y.C. participated in *Tmem163-KO* mouse generation; W.Z. and Q.C. assisted in the design of platelet aggregation assays; T. Li provided technical support for flow cytometry; L.Y. provided technical support for electron microscopy; and X.H. and Y.W. helped analyze mass spectrometry data.

Conflict-of-interest disclosure: The authors declare no competing financial interests.

ORCID profile: W.L., 0000-0002-0248-5510.

Correspondence: Wei Li, Beijing Children's Hospital, Capital Medical University, 56 Nan Li Shi Rd, Xicheng District, Beijing 100045, China; e-mail: liwei@bch.com.cn.

Footnotes

Submitted 2 June 2020; accepted 3 January 2021; prepublished online on *Blood* First Edition 29 January 2021. DOI 10.1182/blood.2020007389.

For original data, please contact the corresponding author.

The online version of this article contains a data supplement.

There is a *Blood* Commentary on this article in this issue.

The publication costs of this article were defrayed in part by page charge payment. Therefore, and solely to indicate this fact, this article is hereby marked "advertisement" in accordance with 18 USC section 1734.

REFERENCES

1. Huizing M, Anikster Y, Gahl WA. Hermansky-Pudlak syndrome and related disorders of organelle formation. *Traffic*. 2000;1(11):823-835.
2. Wei AH, Li W. Hermansky-Pudlak syndrome: pigmentary and non-pigmentary defects and their pathogenesis. *Pigment Cell Melanoma Res*. 2013;26(2):176-192.
3. Dell'Angelica EC, Mullins C, Caplan S, Bonifacino JS. Lysosome-related organelles. *FASEB J*. 2000;14(10):1265-1278.
4. Huizing M, Helip-Wooley A, Westbroek W, Gunay-Aygun M, Gahl WA. Disorders of lysosome-related organelle biogenesis: clinical and molecular genetics. *Annu Rev Genomics Hum Genet*. 2008;9(1):359-386.
5. Swank RT, Novak EK, McGarry MP, Rusiniak ME, Feng L. Mouse models of Hermansky Pudlak syndrome: a review. *Pigment Cell Res*. 1998;11(2):60-80.
6. Wei ML. Hermansky-Pudlak syndrome: a disease of protein trafficking and organelle function. *Pigment Cell Res*. 2006;19(1):19-42.
7. Raposo G, Marks MS, Cutler DF. Lysosome-related organelles: driving post-Golgi compartments into specialisation. *Curr Opin Cell Biol*. 2007;19(4):394-401.
8. Ambrosio AL, Di Pietro SM. Storage pool diseases illuminate platelet dense granule biogenesis. *Platelets*. 2017;28(2):138-146.

9. Chen Y, Yuan Y, Li W. Sorting machineries: how platelet-dense granules differ from α-granules. *Biosci Rep*. 2018;38(5): BSR20180458.

10. Ambrosio AL, Boyle JA, Di Pietro SM. Mechanism of platelet dense granule biogenesis: study of cargo transport and function of Rab32 and Rab38 in a model system. *Blood*. 2012;120(19):4072-4081.

11. Peden AA, Oorschot V, Hesser BA, Austin CD, Scheller RH, Klumperman J. Localization of the AP-3 adaptor complex defines a novel endosomal exit site for lysosomal membrane proteins. *J Cell Biol*. 2004;164(7):1065-1076.

12. Di Pietro SM, Falcón-Pérez JM, Tenza D, et al. BLOC-1 interacts with BLOC-2 and the AP-3 complex to facilitate protein trafficking on endosomes. *Mol Biol Cell*. 2006;17(9): 4027-4038.

13. Reddington M, Novak EK, Hurley E, Medda C, McGarry MP, Swank RT. Immature dense granules in platelets from mice with platelet storage pool disease. *Blood*. 1987;69(5): 1300-1306.

14. Youssefian T, Cramer EM. Megakaryocyte dense granule components are sorted in multivesicular bodies. *Blood*. 2000;95(12): 4004-4007.

15. Hanby HA, Bao J, Noh JY, et al. Platelet dense granules begin to selectively accumulate mepacrine during proplatelet formation. *Blood Adv*. 2017;1(19):1478-1490.

16. Aguilar A, Weber J, Boscher J, et al. Combined deficiency of RAB32 and RAB38 in the mouse mimics Hermansky-Pudlak syndrome and critically impairs thrombosis. *Blood Adv*. 2019;3(15):2368-2380.

17. Meng R, Wang Y, Yao Y, et al. SLC35D3 delivery from megakaryocyte early endosomes is required for platelet dense granule biogenesis and is differentially defective in Hermansky-Pudlak syndrome models. *Blood*. 2012;120(2): 404-414.

18. Chintala S, Tan J, Gautam R, et al. The Slc35d3 gene, encoding an orphan nucleotide sugar transporter, regulates platelet-dense granules. *Blood*. 2007;109(4):1533-1540.

19. Ambrosio AL, Boyle JA, Di Pietro SM. TPC2 mediates new mechanisms of platelet dense granule membrane dynamics through regulation of Ca2+ release. *Mol Biol Cell*. 2015; 26(18):3263-3274.

20. Ambrosio AL, Boyle JA, Aradi AE, Christian KA, Di Pietro SM. TPC2 controls pigmentation by regulating melanosome pH and size. *Proc Natl Acad Sci USA*. 2016;113(20):5622-5627.

21. Zhang Z, Gong J, Sviderskaya EV, Wei A, Li W. Mitochondrial NCKX5 regulates melanosomal biogenesis and pigment production. *J Cell Sci*. 2019;132(14):jcs232009.

22. Apgar J. Effect of zinc deficiency on parturition in the rat. *Am J Physiol*. 1968;215(1):160-163.

23. Emery MP, Browning JD, O'Dell BL. Impaired hemostasis and platelet function in rats fed low zinc diets based on egg white protein. *J Nutr*. 1990;120(9):1062-1067.

24. O'Dell BL, Reynolds G, Reeves PG. Analogous effects of zinc deficiency and aspirin toxicity in the pregnant rat. *J Nutr*. 1977;107(7): 1222-1228.

25. Stefanini M. Cutaneous bleeding related to zinc deficiency in two cases of advanced cancer. *Cancer*. 1999;86(5):866-870.

26. Gordon PR, Browning JD, O'Dell BL. Platelet arachidonate metabolism and platelet function in zinc-deficient rats. *J Nutr*. 1983;113(4): 766-772.

27. Gordon PR, O'Dell BL. Rat platelet aggregation impaired by short-term zinc deficiency. *J Nutr*. 1980;110(10):2125-2129.

28. Gordon PR, Woodruff CW, Anderson HL, O'Dell BL. Effect of acute zinc deprivation on plasma zinc and platelet aggregation in adult males. *Am J Clin Nutr*. 1982;35(1):113-119.

29. Marx G, Krugliak J, Shaklai M. Nutritional zinc increases platelet reactivity. *Am J Hematol*. 1991;38(3):161-165.

30. Taylor KA, Pugh N. The contribution of zinc to platelet behaviour during haemostasis and thrombosis. *Metallomics*. 2016;8(2):144-155.

31. Watson BR, White NA, Taylor KA, et al. Zinc is a transmembrane agonist that induces platelet activation in a tyrosine phosphorylation-dependent manner. *Metallomics*. 2016;8(1): 91-100.

32. Baltaci AK, Yuce K. Zinc transporter proteins. *Neurochem Res*. 2018;43(3):517-530.

33. Costas J. Comment on "current understanding of ZIP and ZnT zinc transporters in human health and diseases". *Cell Mol Life Sci*. 2015;72(1):197-198.

34. Eide DJ. Zinc transporters and the cellular trafficking of zinc. *Biochim Biophys Acta*. 2006;1763(7):711-722.

35. Huang L, Tepaamorndech S. The SLC30 family of zinc transporters: a review of current understanding of their biological and pathophysiological roles. *Mol Aspects Med*. 2013; 34(2-3):548-560.

36. Jeong J, Eide DJ. The SLC39 family of zinc transporters. *Mol Aspects Med*. 2013;34(2-3): 612-619.

37. Kambe T, Hashimoto A, Fujimoto S. Current understanding of ZIP and ZnT zinc transporters in human health and diseases. *Cell Mol Life Sci*. 2014;71(17):3281-3295.

38. Schweigel-Röntgen M. The families of zinc (SLC30 and SLC39) and copper (SLC31) transporters. *Curr Top Membr*. 2014;73: 321-355.

39. Kambe T, Tsuji T, Hashimoto A, Itsumura N. The physiological, biochemical, and molecular roles of zinc transporters in zinc homeostasis and metabolism. *Physiol Rev*. 2015; 95(3):749-784.

40. Yamasaki S, Sakata-Sogawa K, Hasegawa A, et al. Zinc is a novel intracellular second messenger. *J Cell Biol*. 2007;177(4):637-645.

41. Burré J, Zimmermann H, Volknandt W. Identification and characterization of SV31, a novel synaptic vesicle membrane protein and potential transporter. *J Neurochem*. 2007; 103(1):276-287.

42. Barth J, Zimmermann H, Volknandt W. SV31 is a Zn2+-binding synaptic vesicle protein. *J Neurochem*. 2011;118(4):558-570.

43. Cuajungco MP, Basilio LC, Silva J, et al. Cellular zinc levels are modulated by TRPML1-TMEM163 interaction. *Traffic*. 2014;15(11): 1247-1265.

44. Cuajungco MP, Kiselyov K. The mucolipin-1 (TRPML1) ion channel, transmembrane-163 (TMEM163) protein, and lysosomal zinc handling. *Front Biosci*. 2017;22(8):1330-1343.

45. Waberer L, Henrich E, Peetz O, et al. The synaptic vesicle protein SV31 assembles into a dimer and transports Zn^2. *J Neurochem*. 2017; 140(2):280-293.

46. Eichelsdoerfer JL, Evans JA, Slaugenhaupt SA, Cuajungco MP. Zinc dyshomeostasis is linked with the loss of mucolipidosis IV-associated TRPML1 ion channel. *J Biol Chem*. 2010;285(45):34304-34308.

47. Chakraborty S, Vellarikkal SK, Sivasubbu S, Roy SS, Tandon N, Bharadwaj D. Role of Tmem163 in zinc-regulated insulin storage of MIN6 cells: functional exploration of an Indian type 2 diabetes GWAS associated gene. *Biochem Biophys Res Commun*. 2020;522(4): 1022-1029.

48. Sanchez VB, Ali S, Escobar A, Cuajungco MP. Transmembrane 163 (TMEM163) protein effluxes zinc. *Arch Biochem Biophys*. 2019;677: 108166.

49. Li W, Zhang Q, Oiso N, et al. Hermansky-Pudlak syndrome type 7 (HPS-7) results from mutant dysbindin, a member of the biogenesis of lysosome-related organelles complex 1 (BLOC-1). *Nat Genet*. 2003;35(1):84-89.

50. Li W, Rusiniak ME, Chintala S, Gautam R, Novak EK, Swank RT. Murine Hermansky-Pudlak syndrome genes: regulators of lysosome-related organelles. *BioEssays*. 2004; 26(6):616-628.

51. Liu T, Yuan Y, Bai D, et al. Genetic variants and mutational spectrum of Chinese Hermansky-Pudlak syndrome patients. *Pigment Cell Melanoma Res*. 2021;34(1): 111-121.

52. Liu T, Yuan Y, Bai D, et al. The first Hermansky-Pudlak syndrome type 9 patient with two novel variants in Chinese population [published online ahead of print 4 February 2021]. *J Dermatol*. doi:10.1111/1346-8138. 15762.

53. Bultema JJ, Ambrosio AL, Burek CL, Di Pietro SM. BLOC-2, AP-3, and AP-1 proteins function in concert with Rab38 and Rab32 proteins to mediate protein trafficking to lysosome-related organelles. *J Biol Chem*. 2012;287(23): 19550-19563.

54. Gerondopoulos A, Langemeyer L, Liang JR, Linford A, Barr FA. BLOC-3 mutated in Hermansky-Pudlak syndrome is a Rab32/38 guanine nucleotide exchange factor. *Curr Biol*. 2012;22(22):2135-2139.

55. Kloer DP, Rojas R, Ivan V, et al. Assembly of the biogenesis of lysosome-related organelles complex-3 (BLOC-3) and its interaction with Rab9. *J Biol Chem*. 2010;285(10):7794-7804.

56. Ohishi Y, Kinoshita R, Marubashi S, Ishida M, Fukuda M. The BLOC-3 subunit HPS4 is required for activation of Rab32/38 GTPases in

melanogenesis, but its Rab9 activity is dispensable for melanogenesis. *J Biol Chem*. 2019;294(17):6912-6922.

57. Dennis MK, Delevoye C, Acosta-Ruiz A, et al. BLOC-1 and BLOC-3 regulate VAMP7 cycling to and from melanosomes via distinct tubular transport carriers. *J Cell Biol*. 2016;214(3):293-308.

58. Lin HJ, Herman P, Kang JS, Lakowicz JR. Fluorescence lifetime characterization of novel low-pH probes. *Anal Biochem*. 2001;294(2):118-125.

59. Yang Q, He X, Yang L, et al. The BLOS1-interacting protein KXD1 is involved in the biogenesis of lysosome-related organelles. *Traffic*. 2012;13(8):1160-1169.

60. Wei A, Yuan Y, Bai D, et al. NGS-based 100-gene panel of hypopigmentation identifies mutations in Chinese Hermansky-Pudlak syndrome patients. *Pigment Cell Melanoma Res*. 2016;29(6):702-706.

61. Wei A, Yuan Y, Qi Z, et al. Instability of BLOC-2 and BLOC-3 in Chinese patients with Hermansky-Pudlak syndrome. *Pigment Cell Melanoma Res*. 2019;32(3):373-380.

62. White JG. The dense bodies of human platelets: inherent electron opacity of the serotonin storage particles. *Blood*. 1969;33(4):598-606.

63. Caranobe C, Sie P, Boneu B. Serotonin uptake and storage in human platelet density subpopulations. *Br J Haematol*. 1982;52(2):253-258.

64. McNicol A, Israels SJ. Platelet dense granules: structure, function and implications for haemostasis. *Thromb Res*. 1999;95(1):1-18.

65. Gordon N, Thom J, Cole C, Baker R. Rapid detection of hereditary and acquired platelet storage pool deficiency by flow cytometry. *Br J Haematol*. 1995;89(1):117-123.

66. Ramström AS, Fagerberg IH, Lindahl TL. A flow cytometric assay for the study of dense granule storage and release in human platelets. *Platelets*. 1999;10(2-3):153-158.

67. Wall JE, Buijs-Wilts M, Arnold JT, et al. A flow cytometric assay using mepacrine for study of uptake and release of platelet dense granule contents. *Br J Haematol*. 1995;89(2):380-385.

68. Huang L, Kuo YM, Gitschier J. The pallid gene encodes a novel, syntaxin 13-interacting protein involved in platelet storage pool deficiency. *Nat Genet*. 1999;23(3):329-332.

69. Sharda A, Kim SH, Jasuja R, et al. Defective PDI release from platelets and endothelial cells impairs thrombus formation in Hermansky-Pudlak syndrome. *Blood*. 2015;125(10):1633-1642.

70. Ma J, Zhang Z, Yang L, Kriston-Vizi J, Cutler DF, Li W. BLOC-2 subunit HPS6 deficiency affects the tubulation and secretion of von Willebrand factor from mouse endothelial cells. *J Genet Genomics*. 2016;43(12):686-693.

71. Meng R, Wu J, Harper DC, et al. Defective release of α granule and lysosome contents from platelets in mouse Hermansky-Pudlak syndrome models. *Blood*. 2015;125(10):1623-1632.

72. Mahdi F, Madar ZS, Figueroa CD, Schmaier AH. Factor XII interacts with the multiprotein assembly of urokinase plasminogen activator receptor, gC1qR, and cytokeratin 1 on endothelial cell membranes. *Blood*. 2002;99(10):3585-3596.

73. Stadler N, Stanley N, Heeneman S, et al. Accumulation of zinc in human atherosclerotic lesions correlates with calcium levels but does not protect against protein oxidation. *Arterioscler Thromb Vasc Biol*. 2008;28(5):1024-1030.

74. Gorodetsky R, Mou X, Blankenfeld A, Marx G. Platelet multielemental composition, lability, and subcellular localization. *Am J Hematol*. 1993;42(3):278-283.

75. Kiran Gotru S, van Geffen JP, Nagy M, et al. Defective Zn^{2+} homeostasis in mouse and human platelets with α- and δ-storage pool diseases. *Sci Rep*. 2019;9(1):8333.

76. Luzio JP, Hackmann Y, Dieckmann NM, Griffiths GM. The biogenesis of lysosomes and lysosome-related organelles. *Cold Spring Harb Perspect Biol*. 2014;6(9):a016840.

77. Sitaram A, Dennis MK, Chaudhuri R, et al. Differential recognition of a dileucine-based sorting signal by AP-1 and AP-3 reveals a requirement for both BLOC-1 and AP-3 in delivery of OCA2 to melanosomes. *Mol Biol Cell*. 2012;23(16):3178-3192.

78. Newell-Litwa K, Salazar G, Smith Y, Faundez V. Roles of BLOC-1 and adaptor protein-3 complexes in cargo sorting to synaptic vesicles. *Mol Biol Cell*. 2009;20(5):1441-1453.

79. Salazar G, Craige B, Styers ML, et al. BLOC-1 complex deficiency alters the targeting of adaptor protein complex-3 cargoes. *Mol Biol Cell*. 2006;17(9):4014-4026.